Supplemental Material

Electrostatic extension of magnetic proximity effect in $La_{0.7}Sr_{0.3}MnO_3$

Qianqian Lan[1*], Michael Schnedler[1], Lars Freter[1], Chuanshou Wang[2], Kurt Fischer[3], Philipp Ebert[1], and Rafal E. Dunin-Borkowski[1]

[1] Ernst Ruska-Centre for Microscopy and Spectroscopy with Electrons (ER-C 1) and Peter Grünberg Institute (PGI-5), Forschungszentrum Jülich GmbH, 52425 Jülich, Germany

[2] Department of Physics, Southern University of Science and Technology, Shenzhen 518055, People's Republic of China

[3] Department of Mechanical and Electrical Engineering, National Institute of Technology, Tokuyama College, Gakuendai, Shunan, Yamaguchi, 745-8585, Japan

Sample preparation.

The $La_{0.7}Sr_{0.3}MnO_3$ (LSMO) film was grown on a 0.5 wt% Nb-doped $SrTiO_3$ (STO) (001) substrate using pulsed laser deposition. The Mn composition change is associated with an interruption in growth. Specimens were prepared for transmission electron microscopy (TEM) by using focused ion beam milling in an FEI Helios Nanolab 400s dual-beam system. Surface damage was reduced by using Ar ion beam sputtering in a Fischione Nanomill 1040 system. The thickness of the lamella in the electron beam direction was measured to be approximately 120 nm using scanning electron microscopy and determined independently using a log-ratio technique based on electron energy-loss spectroscopy (EELS). In the analysis, the magnetically active thickness was taken to be 110±6 nm in the electron beam direction. It should be noted that the weak thickness change along the growth direction (Fig. S1) is small across the FM/PM transition region and hence does not significantly affect the large magnetization transition at the FM/PM interface investigated here.

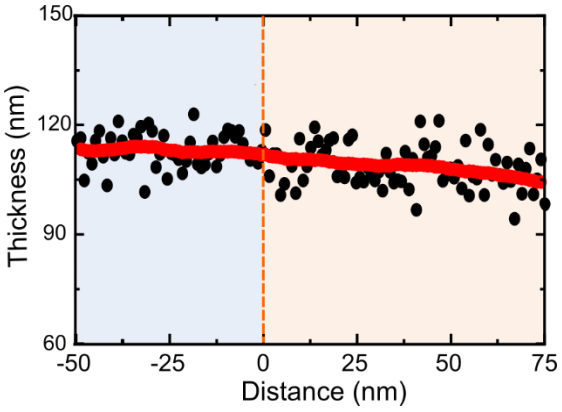

Fig. S1: Thickness measured across the FM/PM interface by EELS using the log-ratio technique vs. distance along growth direction. A slight decrease in thickness is found as a minor effect.

TEM characterization.

The chemical composition and Mn valence state were investigated in an FEI Titan G2 80-200 TEM with a four-quadrant Super-X EDX detector at 200 kV using energy-dispersive X-ray spectroscopy (EDX) and EELS [1]. For the EDX measurement, a probe convergence semi-angle of 24.7 mrad, a probe current of 28.3 pA and a detector collection solid angle of 0.7 sr were used. Maps were recorded at the [010] zone axis. The EDX results were recorded and analysed using Velox software, with a dwell time of 100 µs per pixel and with multiple fast frames accumulated until the sample drifted out of the maximum range for drift compensation. Binning of the experimental data and line profiles (integrating and averaging) was carried out to improve the total signal to noise ratio. Curve fitting by gaussians was then performed. For EELS, a Gatan Enfinium ER (model 977) electron energy-loss spectrometer with DUAL EELS was used. EEL spectra were recorded using a convergence semi-angle of 24.7 mrad and a collection semi-angle of 29 mrad at a dispersion of 0.25 eV per pixel. The energy resolution was 1.25 eV based on the full width at half maximum of the zero-loss peak. Multiple scattering was considered using Fourier-log deconvolution.

For magnetic imaging, off-axis electron holography (EH) was performed in an image-C_S-corrected FEI Titan 80-300 TEM at 300 kV [2]. A liquid-nitrogen-cooled double tilt specimen holder (Gatan model 636) was used to vary the specimen temperature. Off-axis electron holograms were recorded in magnetic-field-free conditions using a direct electron-counting camera (Gatan K2 IS). Maps of the electron optical phase shift φ were reconstructed from off-axis electron holograms digitally using HoloWorks software. The electron optical phase shift contains both electrostatic and magnetic contributions. In order to separate them, the lamella was tilted to 70 in opposite directions parallel to the ferromagnetic/paramagnetic interface and subjected to the magnetic field of the objective lens of the microscope. In each case, the sample was then tilted back to 0° in zero field and the electrostatic and magnetic components were extracted by calculating half of the sum and half of the difference, respectively, between aligned phase images reconstructed from pairs of holograms recorded with opposite magnetization directions in the sample.

The EDX, EELS, and EH results were recorded from the same region of the sample and aligned based on the positions of the LSMO/STO and LSMO/carbon interfaces.

Temperature measurement.

During transmission electron microscopy measurements, the temperature was probed by a Si diode located on the metal plate on which the TEM sample was clamped. Due to the location of the Si diode near the cooling Cu braid and the clamping contact of the sample, the true sample temperature is expected to be slightly higher than the measured value. We anticipate that a measured temperature of 278 K corresponds to a sample temperature close to 280 K. This difference is in line with the observation of a paramagnetic LSMO layer using off-axis electron holography at a nominal temperature of 278 K, despite the fact that T_{C2} was measured to be

279 K using Superconducting Quantum Interference Device measurements. The measured temperature of 278 K was therefore corrected and given as 280±2 K.

Electron holographic tomography.

In order to determine the out-of-plane component of magnetization in the sample, the TEM lamella was rotated with respect to the electron beam direction at 295 K, as shown schematically in Fig. S2. The rotation axis is the *z* axis. Thus, no overlap between the FM and PM layers occurs with rotation angle.

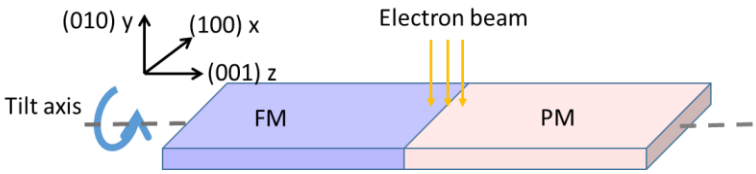

Fig. S2. Schematic diagram showing the tilt axis used for electron holographic tomography. The tilt axis is the *z* axis and the interface is parallel to the *xy* plane. Thus, the electron beam direction is parallel to the FM/PM interface at all sample tilt angles, with no overlap between the FM and PM layers.

Figure S3 shows a right-side view of the lamella in Fig. S2. The phase change induced by the magnetization is given by the expression

$$\frac{\mathrm{d}\varphi}{dx} \sim M_{\mathrm{in}} \cdot d_{\mathrm{eff}} = M \cdot d \cdot cos(\beta) \cdot \big(1 - tan(\beta)tan(\alpha)\big), \qquad (1)$$

where α is the tilt angle of the lamella (during tomographic rotation) and β is the rotation angle of the magnetization away from the in-plane direction. d_{eff} is the effective thickness of the lamella in electron beam direction changing due to tilting. According to Eq. (1), for only in-plane magnetization (i.e. β=0) $\frac{\mathrm{d}\varphi}{dx} \sim M \cdot d$ is constant and independent of the tilt angle α of the lamella.

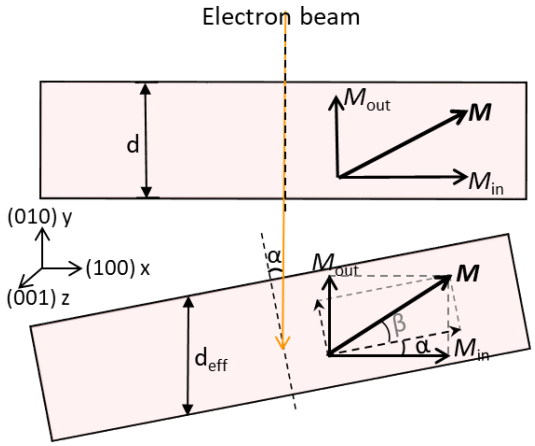

Fig. S3: Schematic cross-section, perpendicular to the rotation axis shown in Fig. S2. The figure illustrates the effect of tilt on the magnetization projected along the electron beam direction. Equation (1) describes the tilt dependence of the gradient of the electron optical phase shift.

Values of $\frac{d\varphi}{dx}$ are plotted in Fig. S4 and are observed to be constant in the FM layer (black dots) and zero in PM layer for every measurement. Based on the error bars and on the absolute values of the measurements, no measurable out-of-plane component of the magnetization was detected. The orientation of the magnetization in the two sublayers is therefore inferred to be in-plane and parallel.

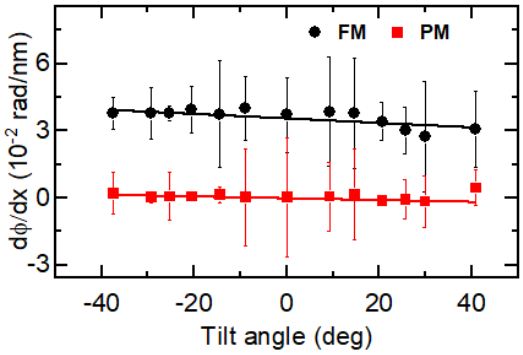

Fig. S4*: Results of electron holographic tomography, showing the gradient of the electron optical phase plotted as a function of tilt angle (with the tilt axis parallel to [001]) in the PM and FM layers at 295 K. The data show that the magnetization has no measurable out-of-plane component.*

1. Ernst Ruska-Centre for Microscopy and Spectroscopy with Electrons (ER-C) et al. (2016). FEI Titan G2 80-200 CREWLEY. Journal of large-scale research facilities. FEI Titan G2 80-200 CREWLEY. *Journal of large-scale research facilities JLSRF* **2,** (2016).

2. Ernst Ruska-Centre for Microscopy and Spectroscopy with Electrons (ER-C) et al. (2016). FEI Titan G2 60-300 HOLO. Journal of large-scale research facilities. FEI Titan G2 60-300 HOLO. *Journal of large-scale research facilities JLSRF* **2,** (2016).